Restoration of microglial function by granulocyte-colony stimulating factor in ALS model mice

Yamasaki, Ryo
Department of Neurology, Neurological Institute, Graduate School of Medical Sciences, Kyushu University

Tanaka, Masahito
Department of Neurology, Neurological Institute, Graduate School of Medical Sciences, Kyushu University

Fukunaga, Mami
Department of Neurology, Neurological Institute, Graduate School of Medical Sciences, Kyushu University

Tateishi, Takahisa
Department of Neurology, Neurological Institute, Graduate School of Medical Sciences, Kyushu University

他

https://hdl.handle.net/2324/26058

Restoration of microglial function by granulocyte-colony stimulating factor in ALS model mice

Ryo Yamasaki, Masahito Tanaka, Mami Fukunaga, Takahisa Tateishi, Hitoshi Kikuchi, Kyoko Motomura, Takuya Matsushita, Yasumasa Ohyagi, Jun-ichi Kira

Department of Neurology, Neurological Institute, Graduate School of Medical Sciences, Kyushu University, Fukuoka, Japan.

Corresponding author: Jun-ichi Kira, Department of Neurology, Kyushu University,

3-1-1 Maidashi, Higashi-ku, Fukuoka 812-8582, Japan.

E-mail: kira@neuro.med.kyushu-u.ac.jp

Phone: +81-92-642-5340

Fax: +81-92-642-5352

Number of figures:	8 figures
Supplemental material:	1 supplemental figure
Number of pages:	35 pages of text
Number of words in abstract:	99 words
Number of words in introduction:	480 words
Number of words in discussion:	1,221 words

1. Introduction

Amyotrophic lateral sclerosis (ALS) is a progressive neurodegenerative disease that affects upper and lower motor neurons. The supposed mechanisms of motor neuron degeneration in ALS include apoptotic cell death, oxidative stress, protein misfolding and aggregation, endoplasmic reticulum stress, and neuroglial inflammation (Agar and Durham, 2003; Consilvio et al., 2004; Kikuchi et al., 2006; Martin, 1999; Menzies et al., 2002; Rakhit et al., 2002); however, the exact mechanisms remain to be elucidated. The majority of ALS cases are sporadic while approximately 5 to 10% of cases are inherited. Among the latter group, about 20% are linked to autosomal dominant mutations in the superoxide dismutase 1 (SOD1) gene (Rosen et al., 1993).

Mutant SOD1 (mSOD1)-transgenic mice exhibit motor neuron degeneration, as seen in human ALS patients (Gurney et al., 1994). Recent studies have demonstrated that high-level expression of mutant SOD1 within all motor neurons and oligodendrocytes, but not in other cell types, substantially delays motor neuron degeneration, indicating an important contribution of cells other than motor neurons and oligodendrocytes (Yamanaka et al., 2008). Among these cells, reducing mutant SOD1 levels in microglia dramatically slowed disease progression (Boillee et al., 2006). Microglia are considered to be heterogeneous and act neuroprotectively on some occasions (Appel et al., 2009). Therefore, it is still unknown whether SOD1 gene mutations make these glial cells neurotoxic or lessen their neuroprotective ability, thereby accelerating neuronal cell death.

Granulocyte colony stimulating factor (G-CSF) is a well-known growth factor for granulocytes, capable of extending the life span of neutrophils by delaying apoptotic cell death (Hu and Yasui, 1997). It acts by binding to a high-affinity receptor (G-CSFR)

expressed on a variety of hematopoietic cells (Avalos, 1996), neurons and glial cells (Tanaka et al., 2006). The role of G-CSF in ALS is yet to be determined. However, we previously measured 16 cytokines and growth factors in the cerebrospinal fluid (CSF) of ALS patients and found G-CSF to be markedly up-regulated (Tanaka et al., 2006). Recently, Pitzer and colleagues (Pitzer et al., 2008) reported neuroprotective effects of G-CSF. However, the contribution of non-neuronal cells to the neuroprotective actions of G-CSF has never been studied.

Therefore, we aimed to clarify the actions of non-neuronal cells, focusing on microglia, following acute and chronic motor neuronal insults, and their responses to G-CSF treatment. First, we used a motor nerve axotomy model as an acute motor neuron injury, in which progression of neuronal degeneration and reactions of non-neuronal cell populations are similar to those observed in ALS (Moran and Graeber, 2004). Second, as a chronic neuronal insult, we studied motor neuron damage and neighboring non-neuronal cell reactions in mSOD1-Tg mice from the presymptomatic stage to the end stage, with and without G-CSF treatment. Third, we analyzed the functions of microglia and macrophages from mSOD1-Tg mice and their responses to G-CSF in culture. Here, we reveal a novel pathway of neuroprotection by G-CSF via functional recovery of microglia.

2. Materials and methods

2.1. Animals.

SOD1G93A [B6SJL-TgN (SOD1-G93A) 1Gur/J; 002726] and SOD1 [B6SJL-Tg (SOD1) 2Gur/J; 002297] mice were acquired from the Jackson Laboratory (Bar Harbor, ME, USA) and bred following institutional approval by the Center of Biomedical Research, Graduate School of Medical Sciences, Kyushu University. These mice were crossed with C57BL/6 females for at least four generations. Transgenic mice were identified using the polymerase chain reaction (PCR) method described previously (Gurney et al., 1994). These animals exhibit a predictable disease onset at about 16 weeks, with leg tremor, decreased stride and muscle strength. Death occurred after approximately 20 weeks. To investigate the systemic side effects of long-term treatment with G-CSF, splenomegaly was assessed by measuring the largest diameter and weight of the spleen.

2.2. Hypoglossal axotomy.

Twelve-week-old male mutant SOD1 (G93A) transgenic (mSOD1-Tg) ALS model mice (n = 20) and their non-transgenic (NTG) littermates (n = 20) were anesthetized with pentobarbital (40 mg/kg, i.p.) and positioned supine; their left hypoglossal nerves, located between the trachea and the sternocleidomastoid muscle, were exposed and then cut with scissors, as described previously (Baba et al., 1999). To avoid spontaneous anastomosis, we cut the nerve at two points (Fig. 1A). These axotomized mice were sacrificed on post-operative (p.o.) days 5, 10, 20, and 40. Each group included mSOD1-Tg mice (n = 5) and NTG littermates (n = 5). All experiments were performed in compliance with the regulations of the Center of Biomedical

Research, Graduate School of Medical Sciences, Kyushu University.

2.3. G-CSF treatment protocol.

To assess the neuroprotective effect of G-CSF in the hypoglossal axotomized model, 12-week-old mSOD1-Tg mice (n = 10) and their NTG littermates (n = 10) were treated with subcutaneous injection of recombinant human G-CSF (Chugai Pharmaceutical, Tokyo, Japan) (200 μg/kg/day) from 5 days before the operation until they were sacrificed. They were sacrificed on p.o. days 20 (n = 5) and 40 (n = 5), and their hypoglossal nuclei were analyzed immunohistochemically.

mSOD1-Tg mice were also grouped into G-CSF-treated (total n = 32) and saline-treated (total n = 31) groups for comparison of life spans. Beginning when mice were 10 weeks old and continuing until death, G-CSF at a dose of 100 μg/kg was injected subcutaneously for five consecutive days per week. The saline group received an equal volume of 0.9% saline solution (NaCl) in parallel. Failure of a mouse to right itself within 30 seconds after being placed on its back in a supine position was scored as "clinical death" (Li et al., 2000).

2.4. Histological analysis of axotomized hypoglossal nuclei and spinal cord.

For the axotomized model, animals were anesthetized with sodium pentobarbital (40 mg/kg, i.p.) 5, 10, 20, and 40 days after the operation (five animals at each time point), and killed by intracardiac perfusion with isotonic saline followed by a chilled fixative consisting of 4% paraformaldehyde (PFA) in 0.2 M phosphate-buffered saline (PBS) (pH 7.4). After perfusion, the brains (including brainstems) were removed and further fixed by immersion in the same fixative overnight at 4°C, and then

immersed in 20% sucrose (pH 7.4) for 24 h at 4°C. Floating axial sections (20-µm thick) of the brainstem were prepared using a cryostat. For double immunofluorescence staining, floating sections of the brainstem, including the hypoglossal nuclei, were stained with the following combinations of primary antibodies for 48 h at 4°C: anti-ionized calcium binding adaptor molecule 1 (Iba1) rabbit polyclonal IgG (dilution, 1:1000, Wako Pure Chemicals Industries, Osaka, Japan) and anti-glial cell line-derived neurotrophic factor (GDNF) mouse monoclonal IgG (dilution, 1:500, Santa Cruz Biotechnology, Santa Cruz, CA, USA); anti-Iba1 mouse monoclonal IgG (1:500, Abcam plc, Cambridge, UK) and anti-brain-derived neurotrophic factor (BDNF; dilution, 1:500, Sigma-Aldrich, MO, USA); anti-Iba1 and fluorescent Nissl stain (dilution, 1:1000; NeuroTrace™, N-21482, Molecular Probes, Eugene, OR, USA); anti-Iba1 and anti-G-CSFR rabbit polyclonal IgG (1:1000, Santa Cruz Biotechnology). After washing with PBS, the sections were incubated with a mixture of secondary antibodies (except for NeuroTrace), 0.5% Alexa 488-conjugated anti-rabbit IgG and Alexa 594-conjugated anti-mouse IgG (Amersham Pharmacia Biotech, Buckinghamshire, UK), for 2 h at room temperature. After several washes with PBS, sections were mounted in Vectashield anti-fading medium (Vector Laboratories, Burlingame, CA, USA) and examined using a confocal laser-scanning microscope (CLSM) (LSM510META, Carl Zeiss, Jena, Germany).

For the analysis of the spinal cords of ALS model mice, after perfusion with 4% PFA, spinal cords were either embedded in paraffin, from which 6-µm sections were prepared, or transferred into 20% buffered sucrose solution for 2 days at 4°C, embedded in O.C.T. compound (Tissue-Tek, Sakura Finetek, Tokyo, Japan), and frozen on dry ice, after which 10-µm sections were prepared. Deparaffinized sections (for G-CSFR) were

dewaxed in xylene followed by rehydration with 100% and 70% ethanol. Sections were

then incubated in 0.3% hydrogen peroxide in absolute methanol for 30 minutes at room

temperature to inhibit endogenous peroxidase. After rinsing in tap water, the sections

were completely immersed in distilled water and heated in 0.01 M citrate buffer (pH

6.0) in a microwave for ten minutes for antigen retrieval. After this pretreatment, the

sections were incubated with anti-G-CSFR rabbit polyclonal antibody (dilution 1:1000,

Santa Cruz Biotechnology)) diluted in 5% non-fat milk (MEIJI, Tokyo, Japan) in 20

mM Tris-HCl (pH 7.6) containing 0.5 M NaCl, 0.05% NaN_3 and 0.05% Tween 20

(TBST) at 4°C overnight, and then with a 1:200 dilution of the appropriate secondary

antibody for 1 hour at room temperature. A colored reaction product was developed

using 3, 3'-diaminobenzidine tetrahydrochloride (DAB) (Sigma-Aldrich) solution

(0.02% DAB, 0.003% H_2O_2, 50 mM Tris-HCl, pH 7.6).

　　　　Frozen sections of spinal cord were collected as described above. Floating

axial sections (20-µm thick) of the spinal cord were prepared using a cryostat. For

double immunofluorescence staining, floating sections of spinal cord were stained with

anti-Iba1 rabbit polyclonal IgG and anti-GDNF mouse monoclonal IgG for 48 h at 4°C.

After washing with PBS, the sections were incubated with a mixture of secondary

antibodies, 0.5% Alexa 488-conjugated anti-rabbit IgG and Alexa 594-conjugated

anti-mouse IgG, for 2 h at room temperature. After several washes with PBS, sections

were mounted in Vectashield anti-fading medium and examined by CLSM for

immunohistochemistry and for the analysis of cell density.

2.5. Quantitative analysis of cell density.

　　　　The modified optical dissector method described previously (Shimizu et al.,

2005) was used for the quantitative measurement of neuron and microglia density in the hypoglossal nucleus and spinal cord. For counting hypoglossal neurons and microglia, six floating sections (20-µm thick) of brainstem, including the hypoglossal nucleus, stained with fluorescent Nissl stain (dilution, 1:1000; NeuroTrace, N-21482, Molecular Probes) for neurons and with anti-Iba1 rabbit polyclonal IgG (dilution 1:1,000) and propidium iodide (dilution, 1:200; P3566, Molecular Probes) for microglia, were randomly selected from each mSOD1-Tg mouse and wild-type littermates with or without G-CSF treatment (n = 4–5 in each group). For counting spinal cord microglia, four floating sections (20-µm thick) of spinal cord stained with anti-Iba1 rabbit polyclonal IgG (dilution 1:1000) and anti-mouse monoclonal GDNF IgG (dilution: 1:500) as described above, from each of the 17-week-old mSOD1-Tg mice with G-CSF treatment (n = 7) and each of the 17-week-old mSOD1-Tg mice without G-CSF treatment (n = 8), were randomly selected and the number of Iba1-positive cells was then counted. The numbers of neurons and microglia on the ipsilateral (operated side (left)) and contralateral sides of the hypoglossal nucleus were counted semi-automatically using the image-analysis software package Image J 1.34 (NIH, Bethesda, USA), command 'Analyze Particle', in each section, and compared statistically as described below. The numbers of neurons and microglia were counted with the examiner blinded to treatment conditions to exclude selection bias.

2.6. Histomorphometry for spinal motor neurons.

The modified optical dissector method was applied for measurement of spinal motor neurons. Briefly, six floating sections (20-µm thick) from fixed L5 spinal cords stained with a fluorescent Nissl stain were randomly selected from each group at 17

weeks (early symptomatic stage). Images of individual sections were captured as a stack at 1-µm step size along the z-direction using a $20 \times$ objective. Each image was transferred to a personal computer, Power Mac G4 (Apple, Cupertino, CA, USA), and analyzed using Image J software version 1.62. Spinal alpha motor neurons were defined based on: (1) the presence of a large single nucleolus located within the nucleus, surrounded by red fluorescent Nissl-stained cytoplasm, and (2) a cell somal area in the range 250–1100 μm^2 (Drachman et al., 2002). Nissl-positive alpha motor neurons consistent with the above criteria were counted semi-automatically by the Image J command 'Analyze Particle'. Numbers of spinal motor neurons were counted with the examiner blinded to treatment conditions to exclude selection bias.

2.7. Axonal histomorphometry.

All mice were anesthetized with pentobarbital intraperitoneally and perfused intracardially with 50 ml of normal saline solution followed by 75 ml of 2.5% (w/v) glutaraldehyde in 0.1 M phosphate-buffered saline (PBS). Spinal cords were dissected and the L5 ventral roots were harvested. These tissues were preserved in 2.5% glutaraldehyde at 4°C for 48 hours, post-fixed in 2% osmium tetroxide for 1 hour, dehydrated through graded ethanol/acetone and then embedded in Epon 812 (TAAB Laboratories Equipment, Berks, UK). Cross sections (0.5 µm) were cut using a Leica RM2255 motorized rotary microtome (Leica, Nussloch, Germany), and stained with 1% toluidine blue (Sigma-Aldrich) and 1% sodium borate (Sigma-Aldrich) in distilled water. Images of L5 axons were captured using a DP12 digital camera (Olympus, Tokyo, Japan) and analyzed using Adobe Photoshop version 6.0 (Adobe Systems, San Jose, CA, USA). Axons from the entire section were then counted, with the examiner blinded to

treatment conditions to exclude selection bias. Data are presented as the number of myelinated axons larger than 4 μm in diameter per whole L5 anterior root.

2.8. Preparation of primary cultured microglia and peritoneal exudate macrophages from mSOD1-Tg mice.

Microglia were isolated from mixed primary cell cultures derived from the cerebral cortices of 3-day-old mSOD1-Tg mice and their NTG littermates according to methods described previously (Yamasaki et al., 2007). After 10 to 14 days in culture, floating cells and weakly attached cells on the mixed glial cell layer were isolated by shaking of the flask. The resulting cell suspension was transferred to a petri dish (Falcon 1001, Lincoln Park, NJ, USA) and allowed to adhere at 37°C. Unattached cells were removed after 30 min, and microglia were isolated as strongly adhering cells. The purity of microglia was more than 96%, as determined by immunostaining for Iba1. Mouse peritoneal exudate macrophages were obtained 3 days after intraperitoneal injection of 2 ml of sterile 4% Brewer thioglycollate medium (Nissui, Tokyo, Japan). The cells were extracted by washing the peritoneal cavity three times with 2 ml of ice-cold PBS. The cells were re-suspended in Dulbecco's modified Eagle's medium (DMEM, Gibco, Invitrogen, CA, USA). They were cultured at 37°C in 5% CO_2 on polystyrene dishes 100 mm in diameter (Corning Glass Works, Corning, NY, USA) at 2×10^6 cells per dish in a total volume of 14 ml. After a 1.5-h adherence period, non-adherent cells were removed by washing three times with 5 ml of PBS pre-warmed to 37°C. Collected microglia and macrophages were treated with G-CSF (2 μg/ml), and cultured for an additional period as described.

2.9. Immunocytochemistry of primary cultured microglia.

Microglial cells were seeded (5×10^4 per well) onto a chamber slide (Nalge Nunc International, NY, USA). Three hours after the cells were seeded, they were fixed with 5% paraformaldehyde (30 min). Following 0.5% Triton-X 100 permeation for 10 min, cells were stained with primary antibody (monoclonal anti-SOD clone SD-G6, Sigma-Aldrich) and then secondary antibodies (Alexa 594-conjugated anti-mouse IgG) according to standard protocols. For the evaluation of phospho-Stat3 nuclear translocation, cells were treated with G-CSF (2 µg/ml) for 12 hours and stained with primary antibody (phospho-Stat3 (Tyr705) antibody, Cell Signaling Technology, MA, USA) and then with secondary antibodies (Alexa 488-conjugated anti-rabbit IgG). The cells were observed by CLSM.

2.10. Cell transmigration assay.

The transmigration ability of microglia was assessed using a Matrigel chamber (Supplementary Fig. 1A). Polycarbonate filters with pores of 8 µm, pre-coated with Matrigel basement membrane matrix (BD Biosciences, NJ, USA) were used. A microglial cell suspension at a density of 200 cells/µl, in serum-free MEM containing 0.3% bovine serum albumin, prepared from mSOD1-Tg mice and their NTG littermates, was plated on cell inserts at a cell density of 1×10^5 per well. All inserts were dipped into lower wells filled with 750 µl of serum-free MEM containing 50 ng/ml monocyte chemotactic protein-1 (MCP-1) (Sigma-Aldrich) and 100 µg/ml adenosine 5'-triphosphate disodium salt (ATP) (Sigma-Aldrich) as chemical attractants. Plates were incubated at 37°C in a 10% CO_2 atmosphere for 22 hours. Cells remaining on the upper surface of the membrane were removed by wiping, and the transmigrated cells

were fixed with 100% methanol (Sigma-Aldrich,) and stained with 1% toluidine blue in 1% sodium tetraborate. The number of microglia that transmigrated to the lower surface of the membrane was manually counted. Each assay was performed in triplicate.

2.11. Immunoblot.

Primary cultured microglia were collected and divided into two groups: an LPS-stimulated group and a control group. The LPS-stimulated group was treated with LPS (100 ng/ml). After 12 hours, cells were collected and used in experiments. The soluble fractions prepared from the collected cell cultures by differential centrifugation were electrophoresed on 10% SDS-polyacrylamide gels. Proteins on SDS gels were transferred electrophoretically at 100 V for 1 hour from the gel to nitrocellulose membranes (Hybond ECL; GE healthcare, Buckinghamshire, UK), and then incubated at 4°C overnight under gentle agitation with primary antibodies against NF-κB p65 (dilution, 1:10,000; Cell Signaling Technology), p-p38 MAPK (dilution, 1:10,000; Cell Signaling Technology) and actin (dilution, 1:10,000; Sigma-Aldrich). After washing, the membranes were incubated with 0.5% horseradish peroxidase (HRP)-labeled donkey anti-rabbit IgG (Amersham). Subsequently, membrane-bound, HRP-labeled antibodies were detected using an enhanced chemiluminescence (ECL) system (GE Healthcare) and a ChemiDoc XRS system (Bio-Rad Laboratories, Hercules, CA, USA).

2.12. Zymography assay.

Matrix metalloproteinase (MMP) enzyme activity was assessed using a zymography assay (Kiaei et al., 2007; Kleiner and Stetler-Stevenson, 1994). Briefly, primary cultured microglia and peritoneal macrophages from both bacterial

lipopolysaccharide (LPS) (100 ng/ml) (Sigma-Aldrich)-stimulated and non-stimulated

mice were collected and resuspended in 1 ml of 50 mM Tris-HCl (pH 7.5), containing

75 mM NaCl and 1 mM phenylmethyl sulfonyl fluoride (PMSF). The homogenates

were then centrifuged at 4°C for 20 minutes at $10,000 \times g$ and the supernatants were

used for zymographic study. The protein concentration of each sample was determined

by the dye-binding method using a protein assay kit with bovine serum albumin as a

standard. The gelatinolytic activity was determined by SDS-PAGE in 7.5%

polyacrylamide gels containing 1 mg/ml gelatin type A (Sigma-Aldrich). Aliquots of

cell homogenate supernatant (30 g/10 µl) were diluted with 50 µl of sample buffer

containing 80 mM Tris-HCl (pH 6.8), 4% SDS and 10% glycerol, and then subjected to

electrophoresis at 25 mA for 90 min at 4°C. After electrophoresis, gels were washed

twice for 30 min in 2% Triton X-100 and incubated for 20 h in incubation buffer (50

mM Tris base, 5 mM $CaCl_2$, 1 µM $ZnCl_2$, 0.01% sodium azide (pH 7.5)) at 37°C. After

incubation, gels were fixed in 20% trichloroacetic acid (Sigma-Aldrich) for 30 min and

stained in 0.5% Coomassie brilliant blue (Sigma-Aldrich) for 90 min. After staining,

gels were destained in 35% ethanol and 10% acetic acid for 60 min. Gelatinolytic

activity was visible as clear bands on a blue background. A standard marker for gelatin

zymography (LL-50007, Life Laboratory Company, Yamagata, Japan) was used to

confirm the identities of gelatinolytic bands on the gels.

2.13. mRNA extraction and real-time reverse transcription (RT)-PCR.

　　　　Primary cultured microglia were isolated and seeded (2×10^5/well) onto 6-well

plates. After 12 h, the cells were treated with each compound and then washed twice

with PBS. Strongly adhered cells were then collected and messenger ribonucleic acids

(mRNAs) were extracted and purified using the RNeasy Mini mRNA purification kit (Qiagen, Tokyo, Japan) according to the manufacturer's protocol. Total RNA (60 ng) was converted to cDNA by reverse transcription using the Transcriptor First Strand cDNA Synthesis Kit (Roche Applied Science, Germany). Aliquots from the reverse transcription reaction mixture were used for PCR amplification. A primer pair designed against glyceraldehyde-3-phosphate dehydrogenase (GAPDH) was used as an internal control. The primer sequences were as follows: GDNF, sense primer (20-mer) 5'-CAAAGTAGGCCAGGCATGTT-3', antisense primer (20-mer) 5'-CCCTTTCTTCGCACTGTAGC-3'; BDNF, sense primer (20-mer) 5'-GCGGCAGATAAAAAGACTGC-3', antisense primer (20-mer) 5'-AAGTTGTGCGCAAATGACTG-3'; G-CSFR, sense primer (22-mer) 5'-CCCCTCAAACCTATCCTGCCTC-3', antisense primer (22-mer) 5'-TCCAGGCAGAGATCAGCGAATG-3'; CCR2, sense primer (20-mer) 5'-ATTCTCCACACCCTGTTTCG-3', antisense primer (20-mer) 5'-CTGCATGGCCTGGTCTAAGT-3'; inducible nitric oxide synthase (iNOS), sense primer (20-mer) 5'-CATGCTAATGCGAAAGGTCA-3', antisense primer (20-mer) 5'-GCTTGTCACCACCAGCAGTA-3'; GAPDH, sense primer (20-mer) 5'-TCCACCACCCTGTTGCTGTA-3', antisense primer (20-mer) 5'-ACCACAGTCCATGCCATCAC-3'. PCR was performed under the following conditions: 94°C for 1 min, 60°C for 1 min and 72°C for 1 min for 30 cycles, followed by a 7 min extension at 72°C. The PCR products (176 bp for GDNF, 495 bp for BDNF, 567 bp for G-CSFR, 192 bp for CCR2, 196 bp for iNOS and 450 bp for GAPDH) were electrophoresed on 1.2% agarose gels and visualized by staining with ethidium bromide. This analysis confirmed that the PCR products were amplified from the original

sequences. The relative intensity of G-CSFR mRNA was determined relative to that of GAPDH mRNA.

Real-time PCR was performed using a SYBR Green real-time PCR Master Mix (Toyobo, Osaka, Japan) and analyzed using a MiniOpticon detection system (Bio-Rad Laboratories). An external standard curve was generated by dilutions of the target PCR products, which had been purified and had their concentrations measured. To confirm amplification specificity, the PCR products were subjected to a melting curve analysis and gel electrophoresis. No other products were amplified because melting curves showed only one peak in each sample. The levels of GDNF and BDNF gene expression in each reaction was normalized to the expressed amounts of GAPDH. The relative mRNA expression levels were calculated according to the comparative CT quantification method.

2.14. Statistical analysis.

Data are expressed as means ± standard error of the mean (SEM). The statistical analyses of data in Figs. 1 and 2 were performed using the Student's t-test. For the data in Figs. 4E, 4G, 6, 7 and 8, a Kruskal-Wallis one-way test was performed; if significance was detected, a Mann-Whitney U test was also performed. Survival evaluation in Fig. 4C was performed by Kaplan-Meier analysis using the log-rank test.

3. Results

3.1. Neuronal degeneration after hypoglossal axotomy and recovery of neuron survival after G-CSF administration

First, we performed left hypoglossal nerve axotomy on 12-week-old mSOD1-Tg mice (n = 20) and NTG mice (n = 20). Forty days after axotomy, the number of Nissl-positive cells on the operated side was lower than that on the unoperated side (Fig. 1A). As shown in Fig. 1B, the viability rate (%) of hypoglossal neurons, calculated as the number of neurons on the operated side divided by the number of neurons on the contralateral side (Zhu et al., 2010), in the NTG mouse hypoglossal nucleus, gradually decreased to 52.2% at 20 days after axotomy, and to about 20% at 40 days after the operation (mean (%) ± SEM: 52.2 ± 3.0 on p.o. day 20, and 19.7 ± 2.3 on p.o. day 40). The decline in the viability of hypoglossal motor neurons on the operated side compared with those on the contralateral side was significantly greater in mSOD1-Tg mice than in NTG mice (mSOD1 vs. NTG = 26.3 ± 3.7 vs. 52.2 ± 3.0, $P = 0.0048$ on p.o. day 20, and 12.4 ± 1.9 vs. 19.7 ± 2.3, $P = 0.0345$ on p.o. day 40).

In the axotomized hypoglossal nucleus, the number of microglia increased, and there were usually two or three microglia around one neuron (Fig. 1Ca-d). This phenomenon became apparent 3 to 5 days after axotomy, and lasted until p.o. day 20. The number of Iba1-postive cells was greater in NTG mice than in mSOD1-Tg mice (microglial cell number on p.o. day 5, operated side ("Ipsi"): NTG vs. mSOD1 (mean ± SEM) = 112.3 ± 10.1 vs. 59.8 ± 6.6, $P = 0.041$; unoperated side ("Contra"): NTG vs. mSOD1 = 8.5 ± 0.9 vs. 6.5 ± 1.0, $P = 0.267$) (Fig. 1Ce). In addition, the cell soma sizes of Iba1-positive cells were also larger in NTG mice than in mSOD1-Tg mice (size of

cell soma (μm^2), mSOD1 vs. NTG = 39.7 ± 3.1 vs. 25.3 ± 0.6, P = 0.016) (Fig. 1Cf).

The Iba1-positive microglia around axotomized motor neurons were immunopositive

for GDNF in both NTG and mSOD1-Tg mice (Fig. 1Da,b); however, they were only

weakly positive for BDNF (Fig. 1Dc,d).

With subcutaneous administration of G-CSF (200 μg/kg/day), following the

protocols shown in Fig. 2A, the viability rate of hypoglossal neurons on the operated

side of the NTG mice increased in both NTG mice and mSOD1-Tg mice on p.o. day 40,

although only in the latter group did this increase reach statistical significance (mean

(%) ± SEM; NTG vs. NTG + G-CSF = 19.7 ± 4.6 vs. 38.5 ± 16.2, P = 0.11, mSOD1-Tg

vs. mSOD1-Tg + G-CSF = 12.4 ± 3.7 vs. 33.0 ± 9.56, P = 0.0194) (Fig. 2B). The

number of Iba1-positive microglia also increased following G-CSF treatment in both

NTG and mSOD1-Tg mice (Fig. 2C). These microglia were G-CSF

receptor-immunopositive (Fig. 3).

3.2. Effects of G-CSF administration on mSOD1-Tg mice

Next, we performed subcutaneous administration of G-CSF (100 μg/kg/day)

following the protocols shown in Fig. 4A. None of the G-CSF-treated mSOD1-Tg mice

died from G-CSF injection itself, or its side effects; however, one mouse died from

bleeding following G-CSF injection. At the time of sacrifice, splenomegaly was present

in all G-CSF-treated mSOD1-Tg mice (n = 7), but no splenomegaly was observed in

saline-treated mice (n = 7) (diameter in cm, 1.9 ± 0.4 vs. 1.5 ± 0.2; weight in mg, 223.3

± 72.4 vs. 122.9 ± 47.4 at 17 weeks) (Fig. 4B). Mild leukocytosis was seen 5 days after

G-CSF treatments; however, leukemia cells were found in neither bone marrow nor

peripheral blood.

Following subcutaneous administration of G-CSF, the life spans of
G-CSF-treated mSOD1-Tg mice became significantly longer than those of
saline-treated mSOD1-Tg mice, as shown by a log-rank test ($P < 0.05$). Mean survival
time increased by 7.6 days among G-CSF-treated mSOD1-Tg mice (141.3 ± 7.1 days, n
= 9) compared with saline-treated mice (133.7 ± 8.1 days, n = 9) (Fig. 4C). The number
of surviving alpha motor neurons in L5 spinal cords of 17-week-old mice (early
symptomatic stage) was slightly higher in G-CSF-treated mSOD1-Tg mice than in
saline-treated controls; however, the difference was not statistically significant (7.4 ±
1.2 vs. 6.6 ± 1.9, $P > 0.1$) (Fig. 4D, E).

To assess the effects of G-CSF on axonal degeneration in mSOD1-Tg mice,
we counted large myelinated axons in the L5 ventral root at different stages of disease
progression, namely, at 12 and 14 weeks (pre-symptomatic stage), and at 17 weeks
(early symptomatic stage). The number of normal large myelinated axons in
G-CSF-treated mSOD1-Tg mice was not significantly different from that in
saline-treated control mice at 12 weeks of age (308 ± 19 vs. 290 ± 10), while at 17
weeks of age significantly more large myelinated axons were preserved in
G-CSF-treated mSOD1-Tg mice compared with saline-treated ones (184 ± 34 vs. 142 ±
30, $P < 0.05$) (Fig. 4F, G).

In the spinal cords of 17-week-old mSOD1-Tg mice, microglia expressing
GDNF were seen adjacent to neurons (Fig. 5). As seen in the hypoglossal nerve
axotomized model, G-CSF also increased microglia recruitment around neurons in this
chronic neuronal damage model, and these microglia expressed GDNF at high levels
(Fig. 5). The number and size of Iba1-positive cells were also increased as seen in the
hypoglossal axotomy model in G-CSF-treated mice (Iba1-positive cell number on 17

weeks old mSOD1-Tg mice; untreated (n = 8) vs G-CSF treated mice (n = 7) (mean ±

SEM) = 62.0 ± 8.8 vs. 118.1 ± 12.6, *P* < 0.05 (Fig. 5J); size of cell soma (μm^2);

untreated vs G-CSF-treated mice = 130.8 ± 6.5 vs. 162.9 ± 7.7, *P* < 0.05) (Fig. 5J).

3.3. Impaired activation and migration of primary cultured microglia from mSOD1-Tg

mice

To elucidate the cause of the impaired microglial reaction in mSOD1-Tg mice,

we next examined the transmigration ability of primary cultured microglia and

peritoneal macrophages *in vitro*. Using ATP (100 μg/ml) as a chemoattractant, the

numbers of NTG and mSOD1-Tg microglia that migrated were significantly greater

than the numbers of non-stimulated microglia that migrated, but the number of

migrating cells was not significantly different between NTG mice and mSOD1-Tg mice,

either in the non-stimulated (mean ± SE, cells per well; NTG vs. mSOD1 = 2.3 ± 0.3 vs.

0.7 ± 0.33) or the activated state (14.3 ± 3.5 vs. 19.7 ± 3.5) (Fig. 6A). To examine the

chemo-attraction response to MCP-1, we first examined mRNA expression for CCR2,

an MCP-1 receptor, in primary cultured microglia from NTG and mSOD1-Tg mice.

Microglia from both NTG and mSOD1-Tg mice expressed CCR2, and there was no

difference in the levels of CCR2 expression between the two, either with or without

G-CSF treatment (Supplementary Fig.1B). Using MCP-1 (50 ng/ml) as the

chemoattractant, the numbers of NTG and mSOD1-Tg microglia that migrated were

also significantly greater than the numbers of non-stimulated microglia that migrated. In

the activated state, the number of migrating cells was significantly lower among

mSOD1-Tg microglia than among NTG microglia (mean ± SE, cells per well; NTG vs.

mSOD1 = 39.3 ± 5.8 vs. 18.7 ± 6.5, *P* < 0.05); however, the numbers in the

non-stimulated state did not differ between the two groups (Fig. 6B). The reduced

migration ability of peritoneal macrophages from mSOD1-Tg mice was even more

remarkable; in the non-stimulated state, the number of migrating cells was significantly

lower among mSOD1-Tg macrophages than among NTG macrophages (mean $\pm$ SE,

cells per well; NTG vs. mSOD1 $= 17.8 \pm 5.6$ vs. 3.3 ± 1.7, $P < 0.05$), while in the

MCP-1-stimulated state, mSOD1-Tg macrophages showed no increase in the number of

migrating cells, resulting in markedly lower migrating cell numbers compared with

NTG macrophages (56.3 ± 30.0 vs. 3.8 ± 3.9, $P < 0.05$) (Fig. 6B). The primary cultured

microglia from mSOD1-Tg mice used for the transmigration assay over-expressed

mSOD1 protein (Fig. 6C).

Because MMP-9 (gelatinase) is an indispensable enzyme for transmigration of

microglia (Choi et al., 2010; Shin et al., 2010), we examined MMP-9 protein levels in

cultured microglia and macrophages with LPS stimulation. The amounts of MMP-9 in

macrophages and microglia were lower in mSOD1-Tg mice than in NTG mice (Fig.

7A-D). Even using LPS-stimulated macrophages and microglia, a reduction in the

enzymatic activities of mSOD1-Tg microglia and macrophages compared with NTG

microglia and macrophages was observed (Fig. 7E). In addition, the levels of

phosphorylation of p38 mitogen-activated protein kinase (MAPK) and nuclear factor κB

(NF-κB) p65 were also lower in mSOD1-Tg macrophages and microglia than in NTG

macrophages and microglia (Fig. 7A-D).

3.4. G-CSF directly affects microglia and restores their migration ability

Finally, we tried to elucidate the direct effects of G-CSF on microglia. When

microglia were treated with G-CSF (2 μg/ml) *in vitro*, the nuclear translocation of

phospho-Stat3 was observed (Fig. 8A). However, the expression levels of GDNF and

BDNF relative to GAPDH (internal control) in G-CSF-treated microglia were not

different from those in non-treated microglia from both mSOD1-Tg and NTG mice (Fig.

8B, C), while migration ability was significantly restored in mSOD1-Tg microglia by

treatment with G-CSF (migrated cell number, mean ± SE, cells per well; NTG vs. NTG

+ G-CSF = 47.0 ± 3.8 vs. 76.0 ± 11.9, $P = 0.074$; mSOD1-Tg vs. mSOD1-Tg + G-CSF

= 31.3 ± 7.0 vs. 119.7 ± 1.5, $P < 0.01$) (Fig. 8D). The expression level of iNOS mRNA

did not differ significantly between microglia with and without G-CSF treatment

(Supplementary Fig. 1B). To determine the levels of G-CSFR mRNA in G-CSF-treated

microglia, we performed RT-PCR for G-CSFR. These microglia expressed G-CSFR

mRNA, but there was no significant difference in the levels of G-CSFR mRNA between

groups (G-CSFR mRNA level relative to GAPDH mRNA level (mean ± SE): NTG =

0.35 ± 0.06, NTG + G-CSF = 0.52 ± 0.07, mSOD1 = 0.40 ± 0.06, mSOD1 + G-CSF =

0.51 ± 0.05, $P > 0.1$) (Fig. 8E).

4. Discussion

The novel findings in the present study, which are likely to relate to the pronounced motor neuron loss, and to the prevention of this loss by G-CSF following acute and chronic neuronal insults in mSOD1-Tg ALS model mice, are as follows: 1) in both acute and chronic neuronal damage models, the increase in the number of microglia expressing GDNF around damaged motor neurons was much weaker in mSOD1-Tg mice than in NTG mice; 2) in an acute motor axotomy model, accelerated neuronal loss was seen even in the pre-symptomatic stage of mSOD1-Tg mice, and microglial reaction after hypoglossal axotomy was successfully restored by subcutaneous injection of G-CSF; 3) chronic administration of G-CSF effectively improved motor axonopathy in mSOD1-Tg mice, in which the number of microglia around damaged neurons was increased; 4) the migration ability of primary cultured microglia and peritoneal macrophages using MCP-1 as a chemoattractant was markedly decreased among mSOD1-Tg cells (also, the levels of the matrix metalloproteinase and activation markers MMP-9, phospho-p38 MAPK and NF-κB p65 were decreased in both microglia and macrophages from mSOD1-Tg mice in which mSOD1 protein was accumulated in the cytoplasm); and 5) microglia from both NTG and mSOD1-Tg mice expressed similar levels of G-CSFR at baseline and after stimulation with G-CSF in culture, whereas, after stimulation with G-CSF, these microglia showed nuclear translocation of phospho-STAT3, and transmigration ability toward the chemokine MCP-1 was restored in mSOD1-Tg microglia.

In the present study, mSOD1-Tg mice demonstrated not only chronic progressive neuronal loss, but also neuronal vulnerability following acute axonal injury, even in the pre-symptomatic stage. Accelerated motor neuron loss in mSOD1-Tg mice

suggests the existence of both an inherent vulnerability of these neurons (Julien, 2001) and unfavorable environments surrounding motor neurons, such as exaggerated neurotoxicity and decreased neuroprotection by other cells (Beers et al., 2006; Boillee et al., 2006; Nagai et al., 2007; Yamanaka et al., 2008). We observed a reduction in the numbers of microglia around neurons in mSOD1-Tg mice in the early phase following acute axotomy. Because the blood–brain barrier has been shown to be intact in the brains of axotomized animals (Raivich et al., 1998), mass influx of blood-borne macrophages is unlikely; therefore, microglial mobilization and activation are assumed to be impaired in mSOD1-Tg mice. However, in the chronic ALS model, it is possible that systemic administration of G-CSF may facilitate mobilization of bone marrow-derived cells into the CNS, as has been shown in Alzheimer's disease model mice (Sanchez-Ramos et al., 2009). These activated microglia around damaged neurons were considered to act neuroprotectively in a rat facial nerve axotomy model (Lopez-Redondo et al., 2000; Moran and Graeber, 2004). Such microglia around damaged neurons were also observed when neurons suffered chronic insults owing to the accumulation of mSOD1 in the symptomatic stages. In our study, microglia around neurons expressed GDNF at high levels and restoration of the microglial response by G-CSF was in accord with the recovery from motor neuron damage following both acute and chronic motor neuron injuries, which also supports a neuroprotective role of these microglia around neurons. We, therefore, suggest that, in mSOD1 mice, an impaired microglial reaction around damaged neurons may contribute to motor neuronal loss following both acute and chronic neuronal insults.

The decrease in microglial reaction around injured neurons in mSOD1-Tg mice is assumed to be caused by decreased migratory and activation abilities. Although

microglia from neonates used in vitro are not the same as adult ones, we found

significant differences in the transmigration ability of even neonatal microglia between

NTG and mSOD1-Tg mice, in association with mSOD1 accumulation, which seems to

relate to the in vivo difference in the microglial response between NTG and mSOD1-Tg

mice. The reduced expression of phospho-p38 MAPK and NF-κB p65 indicated

impaired activation of signal transduction cascades in microglia from mSOD1-Tg mice.

Such impaired migratory and activation abilities were also observed in peritoneal

macrophages, suggesting widespread occurrence of migration and activation defects in

monocyte lineage cells. This decreased migratory ability of primary cultured microglia

was evident following stimulation with MCP-1, but not with ATP, although CCR2

mRNA levels were not decreased in mSOD1-Tg mice compared with those in NTG

mice. MCP-1-induced chemotaxis involves MAPK activation (Ayala et al., 2000), while

ATP-induced chemotaxis via P2Y12 receptors involves Akt activation (Irino et al.,

2008; Ohsawa et al., 2007). We observed a decrease in MAPK activation in mSOD1-Tg

microglia and macrophages, which may well explain the reduction in the migratory

ability of these cells in response to MCP-1 stimulation, but not to ATP stimulation.

Because ATP is released by damaged or hyperactivated neurons and could act as

chemoattractant for microglia *in vivo* (Fields and Stevens, 2000), such ATP release from

mSOD1-Tg motor neurons may be dampened, reflecting motor neuronal dysfunction in

mSOD1-Tg mice (Bruijn et al., 2004; Menzies et al., 2002; Mourelatos et al., 1996).

Alternatively, MCP-1 could be more critical than ATP in microglial mobilization

following motor neuronal injury in mice.

      The observations that microglia express G-CSFR *in vivo* and *in vitro*, and that

nuclear translocation of phospho-STAT3 occurs following stimulation with G-CSF

indicate direct activation of microglia by G-CSF, leading to restoration of the migratory abilities of these cells. Indeed, Zhang and colleagues (Zhang et al., 2009) showed that G-CSF is a powerful chemoattractant for hematopoietic cells, in which activation of JAK1/STAT3 cascades is involved. Since the level of GDNF expression in microglia in culture was not different between NTG and mSOD1-Tg mice, we consider that the restored migratory ability of microglia induced by G-CSF may in part contribute to the enhanced microglial response around damaged motor neurons, and thus, recovery from motor neuron damage, in mSOD1-Tg mice. In addition, although we have so far not obtained any firm evidence suggesting a conversion of microglia from a cytotoxic to a protective phenotype, we consider it necessary to search for evidence for such a possibility, besides the enhancement of migration ability, in the future.

In our study, recovery from motor axon damage was more evident than recovery from motor neuron loss, which may be explained by the observation that, in mSOD1-Tg mice, distal motor axonopathy precedes motor neuronal loss (Fischer et al., 2004). Although Pitzer and colleagues (Pitzer et al., 2008) did not describe occurrences of either splenomegaly or leukocytosis, prolonged administration of G-CSF induced such side effects in our study, which highlights the need for precautions in using the drug for the chronic treatment of ALS in humans.

In summary, we report an impaired microglial response around damaged motor neurons following both acute and chronic neuronal insults in mSOD1-Tg mice, and this impairment appears to contribute to neuronal vulnerability via reduced neurotrophin production in close proximity to damaged motor neurons. Such a dampened response of mSOD1-Tg microglia was effectively restored by G-CSF treatment, which was also associated with recovery from motor neuron and axon

damage. Therefore, in addition to the anti-apoptotic effects of G-CSF as reported (Pitzer et al., 2008), suppression of neuronal degeneration in ALS model mice by G-CSF may result from the restoration of microglial function, particularly their migratory and activation abilities. The results of our study further highlight the importance of microglia in non-cell autonomous cell death of motor neurons in ALS, and the elucidation of this novel mechanism of neuroprotection by G-CSF, via the activation of microglia, may lead to the development of microglial cell-based therapies for ALS.

Acknowledgments

References

Agar, J., Durham, H., 2003. Relevance of oxidative injury in the pathogenesis of motor neuron diseases. Amyotroph Lateral Scler Other Motor Neuron Disord 4, 232-242.

Appel, S.H., Beers, D.R., Henkel, J.S., 2009. T cell-microglial dialogue in Parkinson's disease and amyotrophic lateral sclerosis: are we listening? Trends Immunol 31, 7-17.

Avalos, B.R., 1996. Molecular analysis of the granulocyte colony-stimulating factor receptor. Blood 88, 761-777.

Ayala, J.M., Goyal, S., Liverton, N.J., Claremon, D.A., O'Keefe, S.J., Hanlon, W.A., 2000. Serum-induced monocyte differentiation and monocyte chemotaxis are regulated by the p38 MAP kinase signal transduction pathway. J Leukoc Biol 67, 869-875.

Baba, N., Koji, T., Itoh, M., Mizuno, A., 1999. Reciprocal changes in the expression of Bcl-2 and Bax in hypoglossal nucleus after axotomy in adult rats: possible involvement in the induction of neuronal cell death. Brain Res 827, 122-129.

Beers, D.R., Henkel, J.S., Xiao, Q., Zhao, W., Wang, J., Yen, A.A., Siklos, L., McKercher, S.R., Appel, S.H., 2006. Wild-type microglia extend survival in PU.1 knockout mice with familial amyotrophic lateral sclerosis. Proc Natl Acad Sci U S A 103, 16021-16026.

Boillee, S., Yamanaka, K., Lobsiger, C.S., Copeland, N.G., Jenkins, N.A., Kassiotis, G., Kollias, G., Cleveland, D.W., 2006. Onset and progression in inherited ALS determined by motor neurons and microglia. Science 312, 1389-1392.

Bruijn, L.I., Miller, T.M., Cleveland, D.W., 2004. Unraveling the mechanisms involved in motor neuron degeneration in ALS. Annu Rev Neurosci 27, 723-749.

Choi, M.S., Cho, K.S., Shin, S.M., Ko, H.M., Kwon, K.J., Shin, C.Y., Ko, K.H., 2010. ATP induced microglial cell migration through non-transcriptional activation of matrix metalloproteinase-9. Arch Pharm Res 33, 257-265.

Consilvio, C., Vincent, A.M., Feldman, E.L., 2004. Neuroinflammation, COX-2, and ALS--a dual role? Exp Neurol 187, 1-10.

Drachman, D.B., Frank, K., Dykes-Hoberg, M., Teismann, P., Almer, G., Przedborski, S., Rothstein, J.D., 2002. Cyclooxygenase 2 inhibition protects motor neurons and prolongs survival in a transgenic mouse model of ALS. Ann Neurol 52, 771-778.

Fields, R.D., Stevens, B., 2000. ATP: an extracellular signaling molecule between neurons and glia. Trends Neurosci 23, 625-633.

Fischer, L.R., Culver, D.G., Tennant, P., Davis, A.A., Wang, M., Castellano-Sanchez, A., Khan, J., Polak, M.A., Glass, J.D., 2004. Amyotrophic lateral sclerosis is a distal axonopathy: evidence in mice and man. Exp Neurol 185, 232-240.

Gurney, M.E., Pu, H., Chiu, A.Y., Dal Canto, M.C., Polchow, C.Y., Alexander, D.D., Caliendo, J., Hentati, A., Kwon, Y.W., Deng, H.X., et al., 1994. Motor neuron degeneration in mice that express a human Cu,Zn superoxide dismutase mutation. Science 264, 1772-1775.

Hu, B., Yasui, K., 1997. Effects of colony-stimulating factors (CSFs) on neutrophil apoptosis: possible roles at inflammation site. Int J Hematol 66, 179-188.

Irino, Y., Nakamura, Y., Inoue, K., Kohsaka, S., Ohsawa, K., 2008. Akt activation is involved in P2Y12 receptor-mediated chemotaxis of microglia. J Neurosci Res 86, 1511-1519.

Julien, J.P., 2001. Amyotrophic lateral sclerosis. unfolding the toxicity of the misfolded. Cell 104, 581-591.

Kiaei, M., Kipiani, K., Calingasan, N.Y., Wille, E., Chen, J., Heissig, B., Rafii, S., Lorenzl, S., Beal, M.F., 2007. Matrix metalloproteinase-9 regulates TNF-alpha and FasL expression in neuronal, glial cells and its absence extends life in a transgenic mouse model of amyotrophic lateral sclerosis. Exp Neurol 205, 74-81.

Kikuchi, H., Almer, G., Yamashita, S., Guegan, C., Nagai, M., Xu, Z., Sosunov, A.A., McKhann, G.M., 2nd, Przedborski, S., 2006. Spinal cord endoplasmic reticulum stress associated with a microsomal accumulation of mutant superoxide dismutase-1 in an ALS model. Proc Natl Acad Sci U S A 103, 6025-6030.

Kleiner, D.E., Stetler-Stevenson, W.G., 1994. Quantitative zymography: detection of picogram quantities of gelatinases. Anal Biochem 218, 325-329.

Li, M., Ona, V.O., Chen, M., Kaul, M., Tenneti, L., Zhang, X., Stieg, P.E., Lipton, S.A., Friedlander, R.M., 2000. Functional role and therapeutic implications of neuronal caspase-1 and -3 in a mouse model of traumatic spinal cord injury. Neuroscience 99, 333-342.

Lopez-Redondo, F., Nakajima, K., Honda, S., Kohsaka, S., 2000. Glutamate transporter GLT-1 is highly expressed in activated microglia following facial nerve axotomy. Brain Res Mol Brain Res 76, 429-435.

Martin, L.J., 1999. Neuronal death in amyotrophic lateral sclerosis is apoptosis: possible contribution of a programmed cell death mechanism. J Neuropathol Exp Neurol 58, 459-471.

Menzies, F.M., Ince, P.G., Shaw, P.J., 2002. Mitochondrial involvement in amyotrophic lateral sclerosis. Neurochem Int 40, 543-551.

Moran, L.B., Graeber, M.B., 2004. The facial nerve axotomy model. Brain Res Brain Res Rev 44, 154-178.

Mourelatos, Z., Gonatas, N.K., Stieber, A., Gurney, M.E., Dal Canto, M.C., 1996. The

Golgi apparatus of spinal cord motor neurons in transgenic mice expressing mutant

Cu,Zn superoxide dismutase becomes fragmented in early, preclinical stages of the

disease. Proc Natl Acad Sci U S A 93, 5472-5477.

Nagai, M., Re, D.B., Nagata, T., Chalazonitis, A., Jessell, T.M., Wichterle, H.,

Przedborski, S., 2007. Astrocytes expressing ALS-linked mutated SOD1 release

factors selectively toxic to motor neurons. Nat Neurosci 10, 615-622.

Ohsawa, K., Irino, Y., Nakamura, Y., Akazawa, C., Inoue, K., Kohsaka, S., 2007.

Involvement of P2X4 and P2Y12 receptors in ATP-induced microglial chemotaxis.

Glia 55, 604-616.

Pitzer, C., Kruger, C., Plaas, C., Kirsch, F., Dittgen, T., Muller, R., Laage, R., Kastner,

S., Suess, S., Spoelgen, R., Henriques, A., Ehrenreich, H., Schabitz, W.R., Bach, A.,

Schneider, A., 2008. Granulocyte-colony stimulating factor improves outcome in a

mouse model of amyotrophic lateral sclerosis. Brain 131, 3335-3347.

Raivich, G., Jones, L.L., Kloss, C.U., Werner, A., Neumann, H., Kreutzberg, G.W., 1998.

Immune surveillance in the injured nervous system: T-lymphocytes invade the

axotomized mouse facial motor nucleus and aggregate around sites of neuronal

degeneration. J Neurosci 18, 5804-5816.

Rakhit, R., Cunningham, P., Furtos-Matei, A., Dahan, S., Qi, X.F., Crow, J.P., Cashman,

N.R., Kondejewski, L.H., Chakrabartty, A., 2002. Oxidation-induced misfolding and

aggregation of superoxide dismutase and its implications for amyotrophic lateral

sclerosis. J Biol Chem 277, 47551-47556.

Rosen, D.R., Siddique, T., Patterson, D., Figlewicz, D.A., Sapp, P., Hentati, A.,

Donaldson, D., Goto, J., O'Regan, J.P., Deng, H.X., et al., 1993. Mutations in Cu/Zn

superoxide dismutase gene are associated with familial amyotrophic lateral sclerosis. Nature 362, 59-62.

Sanchez-Ramos, J., Song, S., Sava, V., Catlow, B., Lin, X., Mori, T., Cao, C., Arendash, G.W., 2009. Granulocyte colony stimulating factor decreases brain amyloid burden and reverses cognitive impairment in Alzheimer's mice. Neuroscience 163, 55-72.

Shimizu, T., Hayashi, Y., Yamasaki, R., Yamada, J., Zhang, J., Ukai, K., Koike, M., Mine, K., von Figura, K., Peters, C., Saftig, P., Fukuda, T., Uchiyama, Y., Nakanishi, H., 2005. Proteolytic degradation of glutamate decarboxylase mediates disinhibition of hippocampal CA3 pyramidal cells in cathepsin D-deficient mice. J Neurochem 94, 680-690.

Shin, S.M., Cho, K.S., Choi, M.S., Lee, S.H., Han, S.H., Kang, Y.S., Kim, H.J., Cheong, J.H., Shin, C.Y., Ko, K.H., 2010. Urokinase-Type Plasminogen Activator Induces BV-2 Microglial Cell Migration Through Activation of Matrix Metalloproteinase-9. Neurochem Res.

Tanaka, M., Kikuchi, H., Ishizu, T., Minohara, M., Osoegawa, M., Motomura, K., Tateishi, T., Ohyagi, Y., Kira, J., 2006. Intrathecal upregulation of granulocyte colony stimulating factor and its neuroprotective actions on motor neurons in amyotrophic lateral sclerosis. J Neuropathol Exp Neurol 65, 816-825.

Yamanaka, K., Chun, S.J., Boillee, S., Fujimori-Tonou, N., Yamashita, H., Gutmann, D.H., Takahashi, R., Misawa, H., Cleveland, D.W., 2008. Astrocytes as determinants of disease progression in inherited amyotrophic lateral sclerosis. Nat Neurosci 11, 251-253.

Yamasaki, R., Zhang, J., Koshiishi, I., Sastradipura Suniarti, D.F., Wu, Z., Peters, C., Schwake, M., Uchiyama, Y., Kira, J., Saftig, P., Utsumi, H., Nakanishi, H., 2007.

Involvement of lysosomal storage-induced p38 MAP kinase activation in the overproduction of nitric oxide by microglia in cathepsin D-deficient mice. Mol Cell Neurosci 35, 573-584.

Zhang, Y., Cheng, G., Yang, K., Fan, R., Xu, Z., Chen, L., Li, Q., Yang, A., Jin, B., 2009. A novel function of granulocyte colony-stimulating factor in mobilization of human hematopoietic progenitor cells. Immunol Cell Biol 87, 428-432.

Zhu, L., Lu, J., Tay, S. S. W., Jiang, H., He, B. P., 2010. Induced NG2 expressing microglia in the facial motor nucleus after facial nerve axotomy. Neurosci 166, 842-851.

Figure legends

Fig. 1.

Temporal changes in neuron survival and microglial response following hypoglossal axotomy.

(**A**) Hypoglossal axotomy. (**a**) The hypoglossal nerve (arrow) is located between the sternocleidomastoid muscle and the trachea. The actual skin incision was 3 to 5 mm. (**b**) Non-transgenic (NTG) mouse hypoglossal nucleus on post-operation day 40. (**c**) mSOD1-Tg mice hypoglossal nucleus on post-operation day 40. Nissl stain reveals a loss of hypoglossal neurons on the axotomized (left) side. Compared with the hypoglossal nucleus, the vagal nucleus, located on the dorsal side of the hypoglossal nucleus, remained intact. The loss of hypoglossal neurons is more obvious in mSOD1-Tg mice than in NTG mice. Bar: 100 μm. (**B**) The viability rate of hypoglossal motor neurons on the operated side compared with those on the contralateral side. Means ± SEM are shown. Blank columns represent NTG mice, and filled columns represent mSOD1-Tg mice. Bars: SEM, *: $P < 0.05$, **: $P < 0.01$, n = 5 each. (**C**) Hypoglossal nuclei 5 days after axotomy. Cell nuclei are stained with PI (red) while microglia are immunopositive for Iba1 (green). The microglial response on the operated side of the hypoglossal nucleus is greater in NTG mice (**a**, **b**) than in mSOD1-Tg mice (**c**, **d**). The actual number of Iba1-positive cells on the operated side is lower in mSOD1-Tg mice than in NTG mice (**e**). The cell soma size of Iba1-positive cells is also smaller in mSOD1-Tg mice than in NTG mice (**f**). Bars: SEM, *: $P < 0.05$, n = 4 each. Scale bars in a and c: 80 μm. Scale bar in inset box: 20 μm. (**D**) GDNF-immunopositive microglia in the axotomized hypoglossal nucleus. (**a**, **b**) Iba1 (green) and GDNF (red)

immunoreactivity in the mouse hypoglossal nucleus three days after axotomy. Note the strong immunoreactivity in microglia (yellow). The number of GDNF-positive microglia is fewer in mSOD1-Tg mice than in NTG mice, owing to a decrease in the total number of microglia. (**c**, **d**) Iba1 (red) and BDNF (green) immunoreactivity in the sections adjacent to those shown in (**a**, **b**). BDNF is expressed mainly in neurons, but not in microglia. The background level of BDNF expression in neurons does not appear to be different between mSOD1-Tg mice and NTG mice. Scale bar in **a** and **c**: 50 μm. Scale bar in inset box: 10 μm.

Fig. 2.

Effect of G-CSF administration on axotomized hypoglossal neurons.

(**A**) G-CSF administration protocols. Subcutaneous daily injection of G-CSF (200 μg/kg/day) was started 5 days before axotomy, and continued until the animal was sacrificed. (**B**) The viability rate of hypoglossal motor neurons on the operated side compared with those on the contralateral side was increased by G-CSF treatment in both NTG mice and mSOD1-Tg mice on post-operation day 40 (survival rate (%) ± SEM; NTG vs. NTG + G-CSF = 19.7 ± 4.6 vs. 38.5 ± 16.2, $P = 0.11$, mSOD1-Tg vs. mSOD1-Tg + G-CSF = 12.4 ± 3.7 vs. 33.0 ± 9.56, $P = 0.0194$). (**C**) Hypoglossal nucleus, 5 days after axotomy. **a**: NTG with saline injection, **b**: mSOD1-Tg with saline injection, **c**: NTG with G-CSF injection, **d**: mSOD1-Tg with G-CSF injection. The microglial reaction around damaged neurons is enhanced by G-CSF treatment in both NTG mice (**a, c**) and mSOD1-Tg mice (**b, d**). Compared with NTG mice, such a microglial response is weaker in SOD1-Tg mice with or without G-CSF treatment. Green: Iba1-positive microglia, Red: Nissl-positive neurons. Bars: 50 μm.

Fig. 3.

Expression of G-CSF receptor in microglia.

Hypoglossal nucleus, 3 days after axotomy. (**A–C**) NTG, (**D–F**) NTG + G-CSF, (**G–I**) mSOD1-Tg, and (**J–L**) mSOD1-Tg + G-CSF. (**A, D, G, J**) Iba1 immunostaining, (**B, E, H, K**) G-CSFR immunostaining, and (**C, F, I, L**) merged images. Both in NTG (**A-C**) and mSOD1-Tg (**G-I**) mice, microglia around damaged neurons are all G-CSFR-positive. Following G-CSF treatment, the microglial response is enhanced in both NTG (**D-F**) and mSOD1-Tg (**J-L**) mice, and these microglia are also G-CSFR positive. Green: Iba1-positive microglia. Red: G-CSFR. Bar: 50 μm.

Fig. 4.

Effects of G-CSF administration on the life spans and survival of motor neurons and motor axons in the L5 spinal cords and ventral roots of mSOD1-Tg mice.

(**A**) Schematic illustration of the treatment regimen. Mice were grouped into G-CSF-treated (total n = 32) and saline-treated groups (total n = 31). Beginning when the mice were 10 weeks old and continuing until death, subcutaneous injections of recombinant human G-CSF at a dose of 100 μg/kg were given to the animals for five consecutive days per week. (**B**) At the time of sacrifice, splenomegaly is present in all G-CSF-treated mice. Scale bar = 1 cm. (**C**) The life spans of mSOD1-Tg mice receiving G-CSF treatment are significantly longer than those of saline-treated mSOD1-Tg mice, as shown by the log-rank test ($P < 0.05$). The mean survival time was increased by 7.6 days in G-CSF-treated mSOD1-Tg mice (141.3 ± 7.1 days, n = 9) compared with saline-treated mice (133.7 ± 8.1 days, n = 9). (**D**) Fluorescent Nissl staining of motor

neurons at 17 weeks of age in G-CSF-treated mSOD1-Tg mice and saline-treated control mice. Scale bar = 50 μm. (**E**) The number of surviving alpha motor neurons at 17 weeks (early symptomatic stage) is slightly higher in G-CSF-treated mSOD1-Tg mice than in saline-treated controls; however, there is no significant difference between the two groups (7.4 ± 1.2 vs. 6.6 ± 1.9, $P > 0.1$). G = G-CSF-treated mSOD1-Tg mice. S = saline-treated control mice. NS = not significant. Arrowheads in (**D**) indicate alpha motor neurons. (**F**) Large myelinated axons appear normal at the presymptomatic stage of 12 weeks of age (PS-12) in both G-CSF-treated mSOD1-Tg mice and saline-treated control mice, while in early symptomatic (ES) mice, at 17 weeks of age, large myelinated axons are more abundantly observed in the former than in the latter. Scale bar = 40 μm. (**G**) The number of normal large myelinated axons in G-CSF-treated mSOD1-Tg mice is not significantly different from that in saline-treated control mice at the presymptomatic ages of 12 (PS-12; 308 ± 7.1 vs. 290 ± 10) and 14 weeks (PS-14; 225 ± 17 vs. 205 ± 63). At the early symptomatic stage of 17 weeks of age (ES), significantly more large myelinated axons are found in G-CSF-treated mSOD1-Tg mice than in saline-treated mSOD1-Tg mice (184 ± 34 vs. 142 ± 30, $P < 0.05$). Data are expressed as means ± standard deviation (SD). G = G-CSF-treated mSOD1-Tg mice. S = saline-treated control mice. NS = not significant.

Fig. 5.

Microglial reaction following G-CSF treatment in 17-week-old mSOD1-Tg mice.
Lumbar spinal cords of mSOD1-Tg mice treated with saline (**A, C, D, E**) or G-CSF (**B, F, G, H**). The areas in the square boxes in **A** and **B** are magnified in **C–E** and **F–H**, respectively. Note the robust activation of microglia following G-CSF treatment. As

seen in the axotomized hypoglossal nerve model, G-CSF also enhanced microglial recruitment around neurons in the chronic neuronal damage model, and these microglia expressed GDNF at high levels. Green: Iba1. Red: GDNF. Scale bar in (**A, B**) = 50 μm, (**C–H**) = 10 μm. The actual number of Iba1-positive cells in the G-CSF-treated spinal cords of mSOD1-Tg mice was greater than that in the spinal cords of untreated mSOD1-Tg mice (**I**). The cell soma size of Iba1-positive cells in G-CSF-treated mSOD1-Tg mice was also larger than that in untreated mSOD1-Tg mice (**J**). Bars: SEM, *: $P < 0.05$, n = 8 for G-CSF treated mice, n = 7 for without G-CSF treatment.

Fig. 6.

Migration of primary cultured microglia and peritoneal macrophages from mSOD1-Tg and NTG mice.

(**A**) Chemoattraction with ATP (100 μg/ml). The increase in the number of migrated microglia is not significantly different between mSOD1-Tg microglia and NTG microglia, using ATP as the chemoattractant. A migration assay for peritoneal macrophages with ATP was not performed because the P2Y12 receptor for ATP is not expressed on macrophages. (**B**) Chemoattraction with MCP-1 (50 ng/ml). Although both NTG and mSOD1-Tg mice show significant increases in the numbers of migrating microglia following MCP-1 stimulation, the number of migrating microglia is significantly lower among mSOD1-Tg microglia than among NTG microglia. An even more pronounced decrease in migration ability is observed using peritoneal macrophages from mSOD1-Tg mice. *: $P < 0.05$. Bars: SEM. (**C**) Immunocytochemistry of primary cultured microglia. SOD1 protein is accumulated in

mSOD1-Tg mice microglia. Bar = 50 μm.

Fig. 7.

Immunoblot and gelatin zymography of MMP-9 and immunoblots for NF-κB-p65, p-p38 MAPK and β-actin in peritoneal macrophages and microglia from mSOD1-Tg and NTG mice.

(**A**) Immunoblot analysis of MMP-9, NF-κB-p65, p-p38 MAPK and β-actin in peritoneal macrophages. (**B**) Quantification of the relative immunodensity in (**A**). (**C**) Immunoblot analysis of MMP-9, NF-κB-p65, p-p38 MAPK and β-actin in microglia. (**D**) Quantification of the relative immunodensity in (**C**). *: $P < 0.05$, **: $P < 0.01$. (**E**) Gelatin zymography of MMP-9. MMP-9 enzymatic activity is reduced in both macrophages and microglia from mSOD1-Tg mice when stimulated with LPS, compared with that in macrophages and microglia from NTG mice.

Fig. 8.

Direct activation of microglia by G-CSF administration.

(**A**) Nuclear translocation of phospho-STAT3 in primary cultured microglia following G-CSF treatment. In the absence of G-CSF treatment, phospho-STAT3 is detected mainly in the cytosol in both NTG and mSOD1-Tg microglia. Twelve hours after administration of G-CSF (2 μg/ml), phospho-STAT3 is translocated into the nucleus. Scale bar = 50 μm.

(**B, C**) Microglial levels of GDNF mRNA (**B**) and BDNF mRNAs (**C**) as determined by quantitative real-time RT-PCR, with or without G-CSF treatment. Relative expression levels of GDNF and BDNF in G-CSF-treated microglia were not significantly different

from those in the control group. N.S. = not significant. (**D**) Migration assay with

primary cultured microglia. Migration ability is significantly restored following G-CSF

administration (migrating cell number, mean ± SE, cells per well; NTG vs. NTG +

G-CSF = 47.0 ± 3.8 vs. 76.0 ± 11.9, P = 0.074; mSOD1 vs. mSOD1 + G-CSF = 31.3 ±

7.0 vs. 119.7 ± 1.5, **: P < 0.01). (**E**) Relative expression level of G-CSFR mRNA in

G-CSF-activated primary cultured microglia. These microglia express G-CSFR mRNA,

but there is no significant difference among groups. *: P < 0.05.

Supplementary Fig. 1.

(**A**) Schematic illustration of the migration assay. The 24-well chambers were filled

with 750 µl of DMEM together with MCP-1 (50 ng/ml) or ATP (100 µg/ml). The porous

insert (membrane diameter (Φ) = 9 mm, pore diameter (Φ) = 8 µm) was filled with 500

µl of a cell suspension. Twenty two hours after seeding, the cells on the upper surface of

the pored membrane were removed and migrating cells were counted.

(**B**) Relative levels of CCR2 mRNA, iNOS mRNA and GAPDH mRNA in primary

cultured microglia. Data are presented in triplicate. Microglia from both NTG and

mSOD1-Tg mice expressed CCR2 mRNA and iNOS mRNA at similar levels, either

with or without G-CSF (2 µg/ml).

Fig. 1
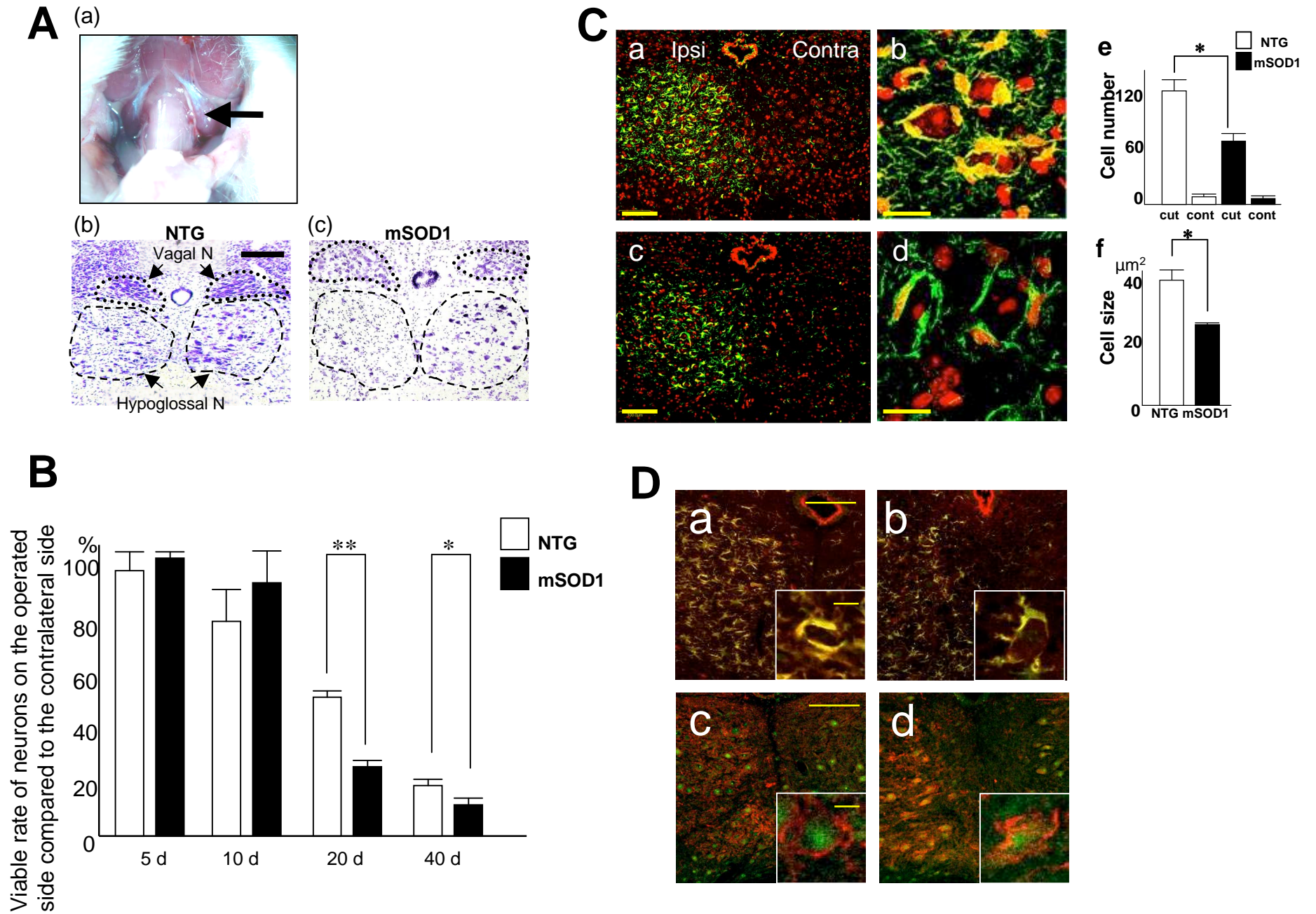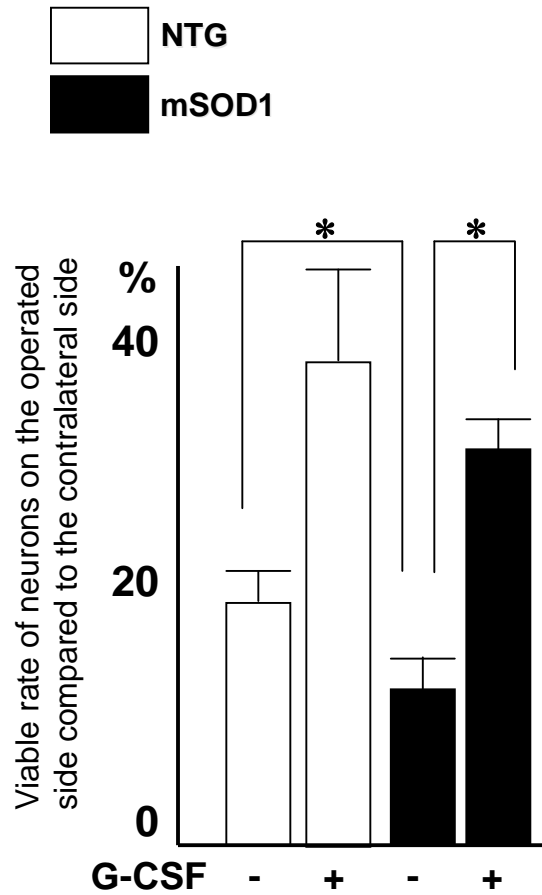
Fig. 2

A

days after operation -5   -4   -3   -2   -1   0   1   2   3..
G-CSF S.C. injection ↓   ↓   ↓   ↓   ↓   ↓   ↓   ↓   ↓ ..
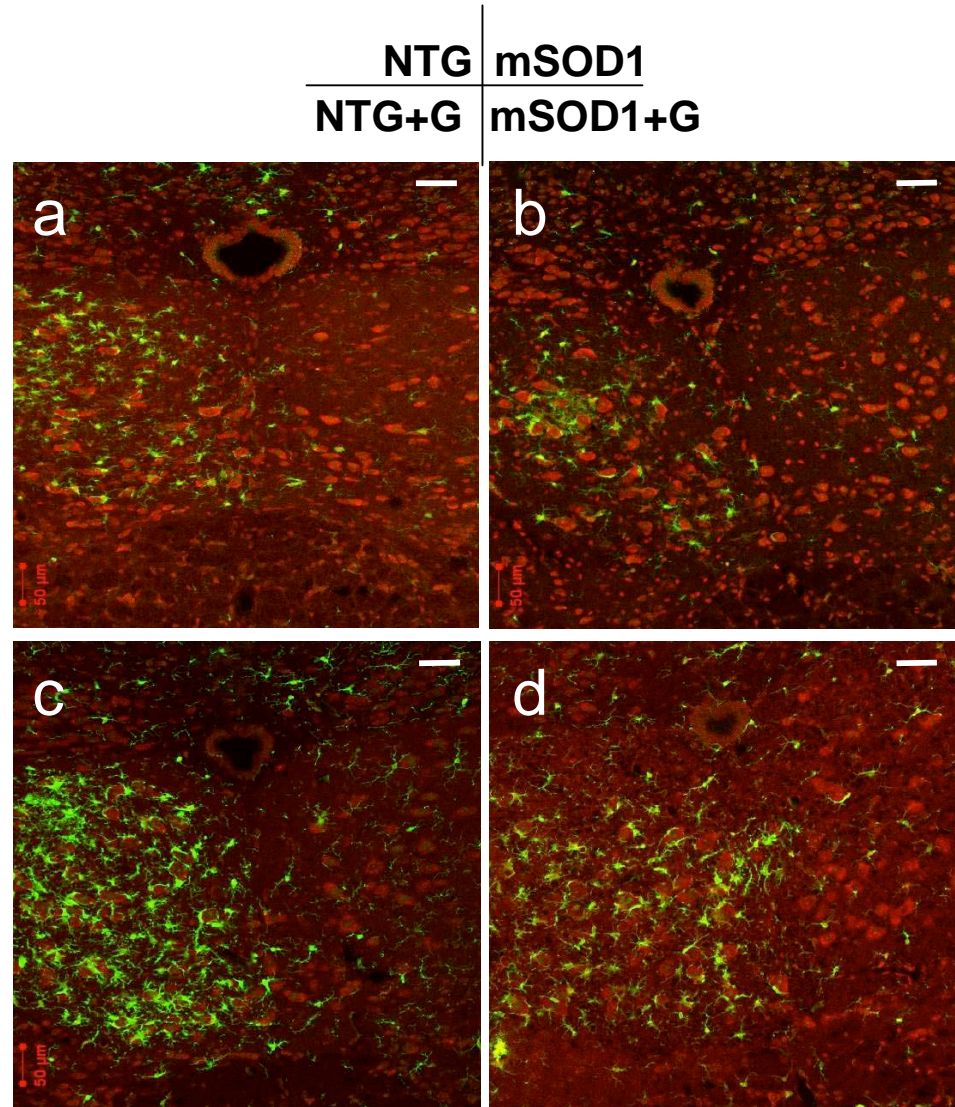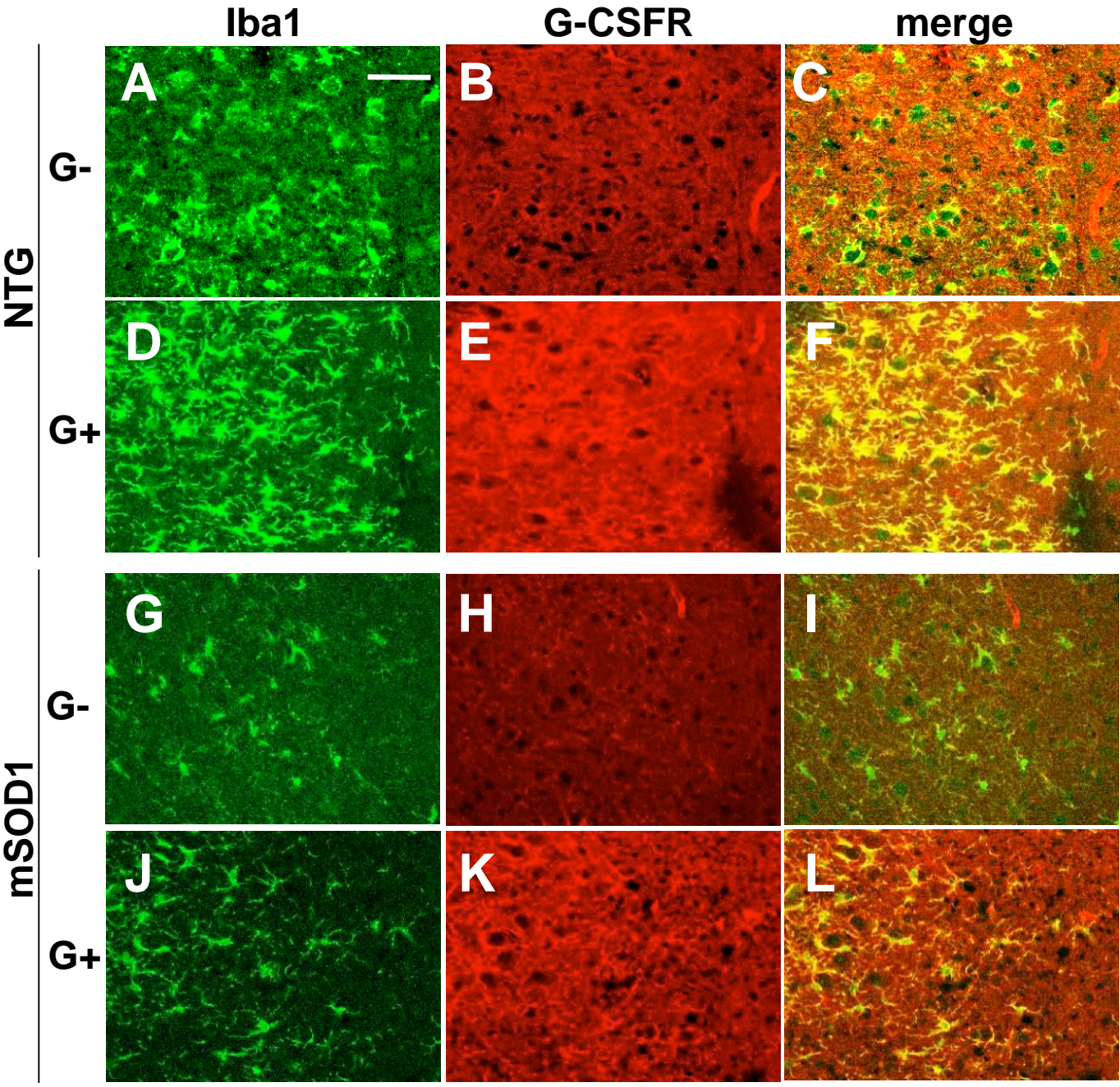(200 µg/kg/day)   CUT

B

C

Fig. 3

Fig. 4

A on-drug period | off-drug period

5 days | 2 days

Subcutaneously injection

Birth

10 weeks
Presymptomatic

End stage

B G-CSF | Saline

1 cm

C

percent survival (%)

G-CSF (n=9)
Saline (n=9)

14 w | 20 w

D G-CSF | Saline

50 μm

E The number of alpha motor neurons

N.S.

12

8

4

0

G S
(n = 3)(n = 3)

F G-CSF | Saline

PS-12

ES

40 μm

G Number of large myelinated axons

N.S. | N.S. | P < 0.05

350
300
250
200
150
100
50
0

G S | G S | G S
(n = 4)(n = 4) | (n = 4)(n = 3) | (n = 7)(n = 7)
PS-12 | PS-14 | PS-17